JOC The Journal of Organic Chemistry

Article

pubs.acs.org/joc

Synthesis and Solvatochromism of Substituted 4-(Nitrostyryl)phenolate Dyes

Rafaela I. Stock, Leandro G. Nandi, Celso R. Nicoleti, Adriana D. S. Schramm, Sheila L. Meller, Renata S. Heying, Daniel F. Coimbra, Karla F. Andriani, Giovanni F. Caramori, Adailton J. Bortoluzzi, and Vanderlei G. Machado*

Departamento de Química, Universidade Federal de Santa Catarina, UFSC, CP 476, Florianópolis, SC, 88040-900, Brazil

Supporting Information

ABSTRACT: 4-(Nitrostyryl)phenols **2a−9a** were synthesized, and by deprotonation in solution, the solvatochromic phenolates **2b−9b** were formed. Their absorption bands in the vis region of the spectra are due to $\pi-\pi^*$ electronic transitions, of an intramolecular charge-transfer nature, from the electron-donor phenolate toward the electron-acceptor nitroarene moiety. The frontier molecular orbitals and natural bond orbitals were analyzed for the protonated and deprotonated forms. The calculated geometries are in agreement with X-ray structures observed for **4a**, **6a**, and **8a**. The HOMO−LUMO energy gaps suggest that, after their deprotonation, an increase in the electron delocalization is observed. In the protonated compounds, the HOMO is primarily localized over the phenol ring and the C═C bridge. After deprotonation, it extends toward the entire molecule, including the NO_2 groups. The solvatochromism of each dye was studied in 28 organic solvents, and it was found that all compounds exhibit a reversal in solvatochromism, which is interpreted in terms of the ability of the media to stabilize their electronic ground and excited states to different extents. The Catalán multiparameter equation is used in the interpretation of the solvatochromic data, revealing that the most important contribution to the solute/solvent interaction is the hydrogen-bond donor acidity of the solvent.

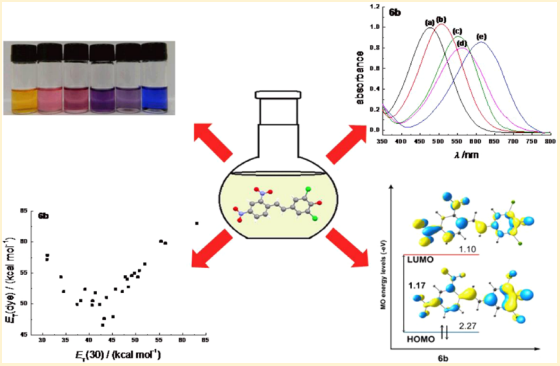

INTRODUCTION

The rate and course of a large number of chemical processes are strongly dependent on the solvent used.[1−5] The choice of solvent (or a mixture of solvents) based on certain criteria represents a variable which is fundamental for the purification and separation of organic compounds. The presence of contaminants in the solvent in very small amounts can strongly influence the yield in many organic reactions. It is also known that the medium can strongly affect the spectrometric data of the dissolved compounds, such as their emission and absorption bands.[1,2,5] These effects are commonly attributed to the solvent polarity, which is defined as the overall solvating ability of the medium.[1,5] Many solvent polarity scales have been proposed to explain the solvent-dependent chemical processes. Several of these polarity scales are based on the use of solvatochromic compounds.[1,2,5,6] For these probes, the position and/or intensity of the bands in the visible region is modified when the solvent polarity is changed.[1,5]

The very popular $E_T(30)$ solvent polarity scale is based on the use of Reichardt's pyridinium *N*-phenolate betaine dye, 2,6-diphenyl-4-(2,4,6-triphenylpyridinium-1-yl)phenolate (compound **1**; see Scheme 1), and its derivatives.[1,5,7−9] These zwitterionic dyes exhibit a strong negative solvatochromism due to their solvent-dependent vis band, with a strong charge-transfer character. A negative solvatochromism occurs when the solvatochromic band is hypsochromically shifted with an increase in the polarity of the solvent.[1]

Scheme 1. Molecular Structures of Pyridinium *N*-Phenolate Betaine Dye 1 and Compounds 2a−9a, as Well as Their Corresponding Phenolates 2b−9b

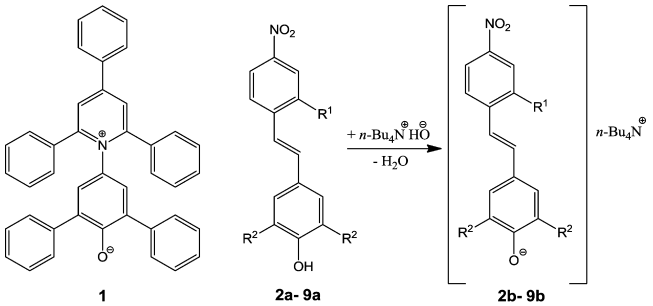

	2a, b	3a, b	4a, b	5a, b	6a, b	7a, b	8a, b	9a, b
R^1	NO_2	H	NO_2	H	NO_2	H	NO_2	H
R^2	H	H	Br	Br	Cl	Cl	CH_3	CH_3

Received: April 30, 2015
Published: July 24, 2015

DOI: 10.1021/acs.joc.5b00983
J. Org. Chem. 2015, 80, 7971−7983

Pyridinium *N*-phenolate dye **1** has inspired many research groups to design other families of solvatochromic dyes. In general, the solvatochromic dyes exhibiting negative solvatochromism have an electron-donor phenolate group in their molecular structure and a pyridinium center as the electron-acceptor group.[10−22] Recently, the solvatochromism of nitro-substituted benzylideneaminophenolates was investigated by our group.[23] These compounds have phenolate donor groups and 4-nitro- or 2,4-dinitrophenyl acceptor groups connected by means of a conjugated C═N bridge. These compounds exhibit a reverse solvatochromism: a decrease in the molar transition energy (E_T) values for these dyes was found on changing the solvent from the most polar solvent (i.e., water) to *N*,*N*-dimethylacetamide (DMA). However, the E_T(dye) values increase for solvents with $E_T(30)$ values below 42.9 kcal mol^{-1} until the least polar solvent (*n*-hexane) used in the studies. Reverse solvatochromism has been documented over the past four decades[24] in several investigations involving solvatochromic cyanines and merocyanines.[15,21,25−29] This phenomenon has been explained on the basis of (a) dye aggregation in low polarity solvents,[10,12,28] (b) solvent-dependent *cis*−*trans* (*E*/*Z*) isomerization processes,[30,31] and, most commonly, (c) the different abilities of polar and nonpolar solvents to stabilize the electronic ground and excited states of the probe.[23,27,32,33]

The focus of the study reported herein was the design of novel solvatochromic dyes with a conjugated C═C bridge in their molecular structure. The main interest was to verify the role of the conjugated bridge in the level of solvatochromism observed for these compounds, through comparison with previously prepared analogous imines.[23] In this regard, we report herein the synthesis and characterization of compounds **2a**−**9a** (Scheme 1). The deprotonation of these compounds generates the solvatochromic dyes **2b**−**9b**, which were studied in 28 solvents. The influence of an additional nitro group on the solvatochromic properties of the dyes was investigated. In addition, the importance of the conjugated C═C bridge in relation to the level of the solvatochromism exhibited by these systems is discussed. Multiparametric analysis of the experimental data was also carried out in order to verify the contribution of various solvent parameters to the solvatochromism exhibited by the probes.

RESULTS AND DISCUSSION

Synthesis of the Compounds. Compounds **2a**−**8a** were synthesized as shown in Scheme 2A through condensation of

Scheme 2. Preparation of Compounds 2a−9a

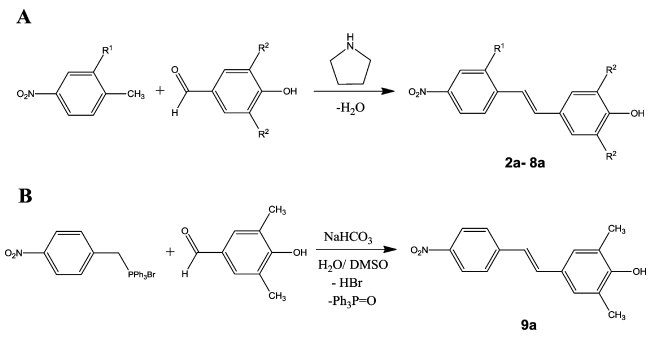

4-nitrotoluene or 2,4-dinitrotoluene with the corresponding aldehyde in the presence of pyrrolidine. Pyrrolidine acts as a base, abstracting a proton from the nitroarene and providing the carbanion, which carries out a nucleophilic attack on the aldehyde carbonyl, generating a tetrahedral intermediate. The latter undergoes water elimination to form the substituted stilbene. The products of the reactions were obtained in yields of 19−51%. Low yields obtained in reactions to afford stilbenes through condensation reactions have been reported in the literature.[34,35] In addition, the highest yields were obtained for the products containing 2,4-dinitrophenyl groups, due to the fact that 2,4-dinitrotoluene is appreciably more acidic than 4-nitrotoluene. Compound **9a** could not be obtained through this methodology. Therefore, this stilbene was synthesized by means of the Wittig reaction (Scheme 2B), reacting (4-nitrobenzyl)triphenylphosphonium bromide[36] with 3,5-dimethyl-4-hydroxybenzaldehyde in the presence of sodium hydrogen carbonate.

The compounds were purified through column chromatography and/or recrystallization, and the characterizations showed that their purity was adequate for the spectroscopic studies. Stilbenes **4a**, **6a**, **7a**, and **8a** are novel compounds and were characterized using IR, ^{1}H NMR, and HRMS techniques. Only the ^{13}C NMR spectrum of **7a** was obtained, due to the low solubility of the other compounds. Monocrystals of compounds **4a**, **6a**, and **8a** were obtained, allowing their structural characterization through X-ray diffraction.

X-ray Structure of Compounds 4a, 6a, and 8a. Figure 1 shows the molecular structures for **4a**, **6a**, and **8a**. Compounds **4a** and **6a** crystallize in the monoclinic system (space group $P2_1/c$), while compound **8a** crystallizes in the triclinic mode, space group $P\bar{1}$. Their main bond distances and torsion angles are reported in Tables S7−S15 (Supporting Information). The crystallographic data show that all compounds have an (*E*)-configuration. It can be observed in Table 1 that the length of the C═C bond in the three compounds analyzed is compatible with those of conjugated systems where aromatic groups are connected via a C═C bridge. The interplanar angles between donor and acceptor groups vary depending on the groups in the 2,6-positions of the phenol moieties. Compounds **4a** and **6a**, which have bromine and chlorine atoms as substituents, exhibit interplanar angles between the mean plane of the aromatic rings of 25.02° and 36.6°, respectively. For compound **8a**, with methyl groups, this angle is very small (0.82°). The interplanar angles between the acceptor ring and the nitro group at position 4 are smaller than that at position 2 for **4a** and **8a**, suggesting a considerable steric hindrance at the *ortho* position.

Solvatochromism of Dyes 2b−9b and Theoretical Calculations. Solutions of **2a**−**9a** are pale yellow, but after deprotonation dyes **2b**−**9b** are generated, which exhibit different colors, as shown in Figure 2. For instance, solutions of dye **6b** are yellow in water, rose in toluene, red-violet in benzyl alcohol, violet in acetonitrile, lilac in acetone, and blue in DMF. The solvatochromism was confirmed through the changes observed in the UV−vis spectra of the dyes when the polarity of the medium was altered. Figure 3 shows the UV−vis spectra for dyes **2b**−**9b** in some selected solvents. For instance, dye **5b** in water exhibits an absorption band with a maximum at 424 nm. This band is shifted to λ_{max} = 454 nm in ethanol, while, in dichloromethane, diethyl ether, and DMA, the band maximum is displaced to 484, 476, and 534 nm, respectively. The bands in the vis region of the spectra are due to $\pi-\pi^*$ electronic transitions, with an intramolecular charge transfer from the electron-donor phenolate moiety toward the electron-acceptor 4-nitrophenyl (or 2,4-dinitrophenyl) moiety.

The frontier molecular orbitals and natural bond orbitals (NBOs), including second-order perturbation analysis of the

DOI: 10.1021/acs.joc.5b00983
J. Org. Chem. 2015, 80, 7971−7983

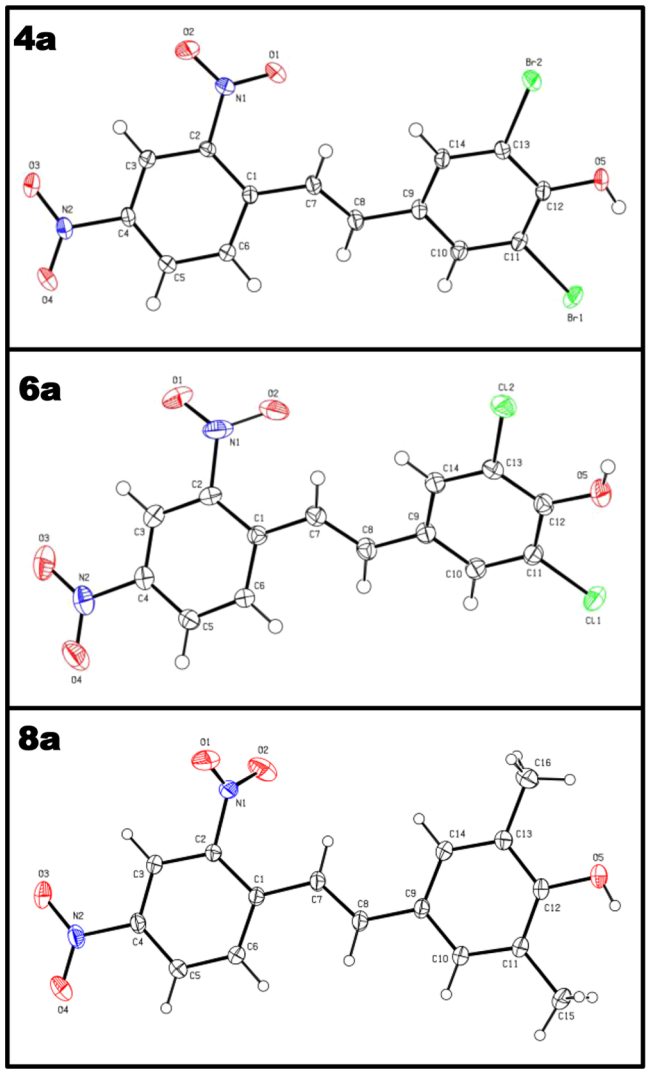

Figure 1. Molecular structures of compounds **4a**, **6a**, and **8a**. Displacement ellipsoids are drawn at the 40% probability level.

Table 1. Interplanar Angles and C═C Bond Lengths for Compounds 4a, 6a, and 8a Obtained from the Crystallographic Data

compound	C═C bond length [Å]	interplanar angle between donor and acceptor ring [deg]	interplanar angle of the nitro group at position 2 [deg]	interplanar angle of the nitro group at position 4 [deg]
4a	1.3350 (2)	25.02 (3)	17.7 (1)	5.80 (9)
6a	1.3379 (13)	36.60 (2)		5.40 (7)
8a	1.3414 (15)	0.82 (3)	67.04 (6)	2.14 (13)

Fock matrix to estimate donor−acceptor interactions, were analyzed for the protonated (**2a**−**9a**) and deprotonated analogues (**2b**−**9b**). The same analysis was extended to analogues of **2a**−**3a** and **2b**−**3b** containing C═N conjugated bridges in order to provide information on the differences in the electronic structures of the two types of bridges. The geometries calculated were validated by comparison with X-ray structures available for **4a**, **6a**, and **8a**. The geometries obtained are in excellent agreement with the X-ray data, as indicated by selected parameters reported in Figures S51 and S52 (Supporting Information). For instance, the C═C bond lengths calculated

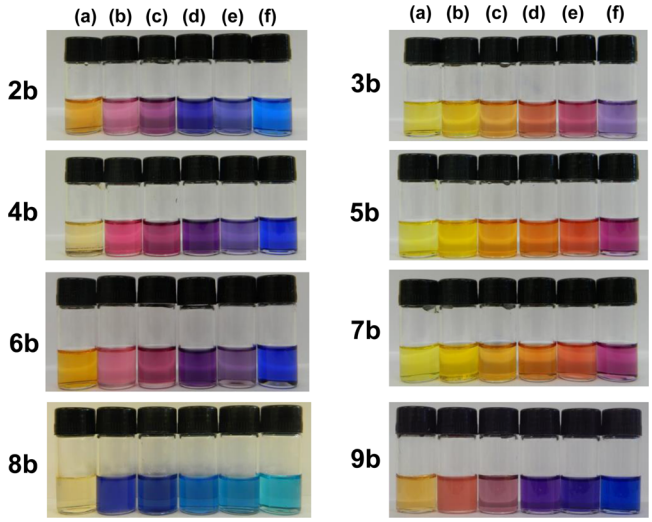

Figure 2. Color of solutions of **2b**−**9b** in water (a), toluene (b), benzyl alcohol (c), acetonitrile (d), acetone (e), and DMF (f).

(and obtained from the crystallographic data) for **4a**, **6a**, and **8a** are 1.356 (1.335), 1.356 (1.338), and 1.360 (1.341) Å, respectively. In general, calculated bond lengths are slightly longer when compared with X-ray data, which can be attributed to the crystal-packing effect. The geometries calculated indicate that the chemical bonds connecting donor and acceptor rings, C(1)−C(7)═C(8)−C(9) (Figure 1), present a very particular behavior. In compounds **2a**−**9a**, the double-bond character of C(7)═C(8) is very pronounced. However, after deprotonation to give **2b**−**9b**, the C(7)═C(8) bond is longer, while the C(1)−C(7) and C(8)−C(9) are shorter, indicating an increase in the electron delocalization between the two aromatic moieties after the deprotonation (Figures S51 and S52, Supporting Information). The results also show that the C(1)−C(7)═C(8)−C(9) bond lengths in **2a**−**9a** or in **2b**−**9b** are not dependent on the number of NO_2 groups or on the nature of substituents employed. A similar trend, in terms of C(1)−C(7)═C(8)−C(9) bond lengths, was observed for the corresponding analogues of **2a**−**3a** and **2b**−**3b**, named **2a-im**, **3a-im**, **2b-im**, and **3b-im**, which contain the C═N (instead of C═C) bridge. The C(1)−C(7)═N(8)−C(9) bond lengths reveal that, as expected, the bond distances for C═N are shorter than those for C═C. The comparison of **2a-im** with **2b-im** and of **3a-im** with **3b-im** verifies that the C(7)═N(8) bond lengths become longer, while, in the cases of C(1)−C(7) and N(8)−C(9), they become shorter (Figure S53, Supporting Information).

Figure 4 shows the frontier molecular orbital plots for **2a**−**3b** as well as the eigenvalues and HOMO−LUMO gaps for all compounds (**2a**−**9b**). According to Figure 4, the HOMO−LUMO energy gaps suggests that, after deprotonation, there is an increase in the electron delocalization, which is entirely in line with the calculated geometrical parameters. It is evident that the energy gaps for **2a**−**9a** are larger than those for **2b**−**9b**. For instance, moving from **2a** to **2b**, the gap decreases from 1.88 to 1.21 eV. This is consistent with the orbital plots, indicating that, in **2a** and **3a**, the HOMO is primarily localized over the phenol ring and the C═C bridge. On the other hand, after deprotonation, it extends toward the entire molecule, including the NO_2 groups. A similar qualitative trend is observed for the analogues **2a-im** to **3b-im** (Figure 5). In order to quantitatively evaluate the electron delocalization over the C═C bridges, the second-order perturbation analysis of the

DOI: 10.1021/acs.joc.5b00983
J. Org. Chem. 2015, 80, 7971−7983

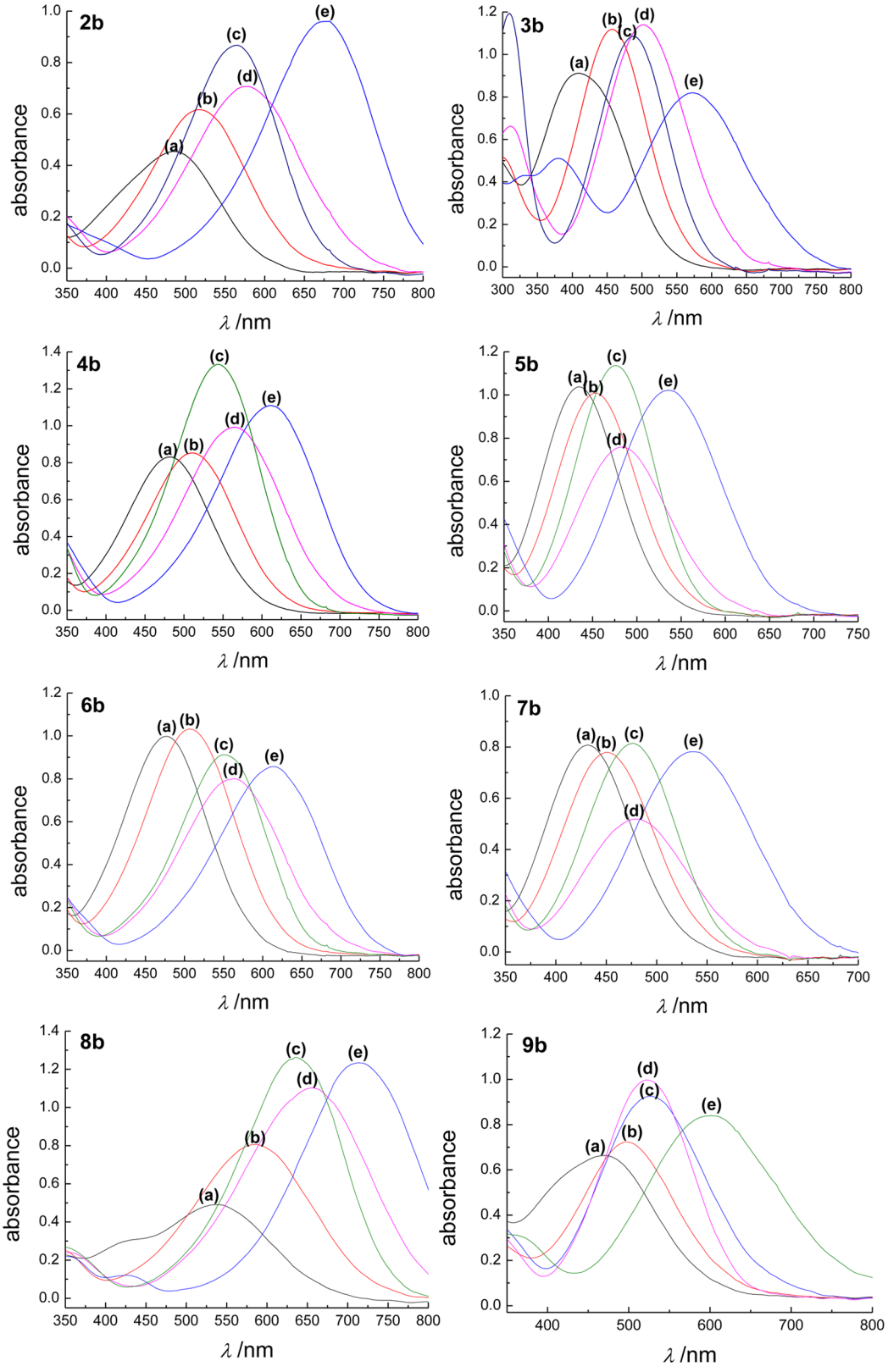

Figure 3. UV−vis spectra of **2b**−**9b**, dissolved in methanol (a), ethanol (b), dichloromethane (c), diethyl ether (d), and DMA (e).

Fock matrix was performed. The results show that the electron delocalization over the C═C bridge provides significant energy stabilization for both sets of compounds, that is, **2a**−**9a** and **2b**−**9b** (Tables S16−S31, Supporting Information, and Figure 6). After the deprotonation to **2b**−**9b**, an increase in the quantity and magnitude of donor−acceptor stabilizing interactions is observed for all compounds. In fact, electron donation is observed from occupied NBOs located at the C═C bond toward unoccupied NBOs inboth rings. For instance, the interactions $\pi_{C7\text{-}C8} \rightarrow \pi^*_{C1\text{-}C2}$ and $\pi_{C7\text{-}C8} \rightarrow \pi^*_{C9\text{-}C10}$ provide stabilizations not only for

DOI: 10.1021/acs.joc.5b00983
J. Org. Chem. 2015, 80, 7971−7983

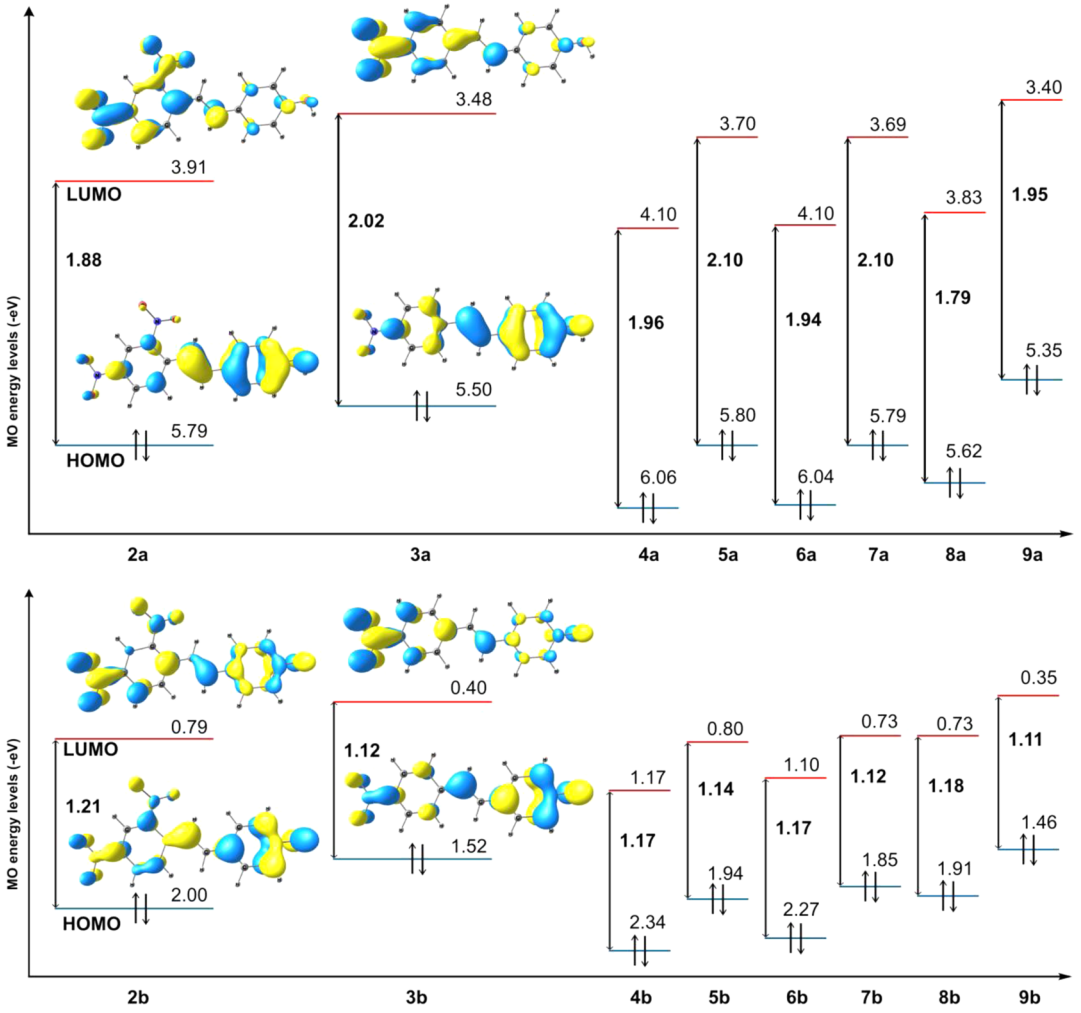

Figure 4. Contour plots for compounds **2a**, **3a**, **2b**, and **3b** and energies of the frontier orbitals (HOMO and LUMO) for compounds **4a**–**9a** and **4b**–**9b**. Contour plots for **4a**–**9b** are shown in Figures S54 and S55 (Supporting Information).

protonated (**2a**–**9a**) but also for deprotonated (**2b**–**9b**) species, ranging from 12.71 to 15.05 kcal mol^{-1} and from 11.33 to 11.76 kcal mol^{-1}, respectively (Tables S16–S31, Supporting Information, and Figure 6). Donor–acceptor interactions are also observed in the opposite direction, that is, from occupied NBOs in both rings to the $\pi^*_{C7\text{-}C8}$ orbital at the C=C bridge ($\pi_{C1\text{-}C2} \rightarrow \pi^*_{C7\text{-}C8}$ and $\pi_{C9\text{-}C10} \rightarrow \pi^*_{C7\text{-}C8}$). In this case, the most stabilizing interactions come from the phenol and phenolate rings toward the bridges ($\pi_{C9\text{-}C10} \rightarrow \pi^*_{C7\text{-}C8}$), presenting stabilization energy values ranging from 14.84 to 21.85 kcal mol^{-1} (Tables S16–S31, Supporting Information), while the donor–acceptor interactions involving occupied NBOs located in the rings containing NO_2 groups and unoccupied NBOs of the C=C bridges ($\pi_{C1\text{-}C2} \rightarrow \pi^*_{C7\text{-}C8}$) provide energy stabilization values ranging from 9.74 to 14.58 kcal mol^{-1}. A comparison between the nitro and the dinitro groups for **2a**–**9a** compounds shows that the additional nitro substituent decreases the magnitude of the $\pi_{C7\text{-}C8} \rightarrow \pi^*_{C1\text{-}C2}$ and $\pi_{C9\text{-}C10} \rightarrow \pi^*_{C7\text{-}C8}$ interactions, while an increase in the $\pi_{C7\text{-}C8} \rightarrow \pi^*_{C9\text{-}C10}$ and $\pi_{C1\text{-}C2} \rightarrow \pi^*_{C7\text{-}C8}$ interactions is observed. On the other hand, for the deprotonated species **2b**–**9b**, this trend is not observed; the energy stabilizations that stem from $\pi_{C7\text{-}C8} \rightarrow \pi^*_{C1\text{-}C2}$ and $\pi_{C7\text{-}C8} \rightarrow \pi^*_{C9\text{-}C10}$ donor–acceptor interactions decrease, while the $\pi_{C1\text{-}C2} \rightarrow \pi^*_{C7\text{-}C8}$ and $\pi_{C9\text{-}C10} \rightarrow \pi^*_{C7\text{-}C8}$ interactions are more stabilizing. The same type of donor–acceptor interactions is less stabilizing in analogues containing C=N, **2a-im** to **3b-im**. The NBO results also show that the presence of electron-donating or electron-withdrawing substituents in the phenol/phenolate ring does not cause a significant change in the magnitude of the $\pi_{C7\text{-}C8} \rightarrow \pi^*_{C1\text{-}C2}$, $\pi_{C7\text{-}C8} \rightarrow \pi^*_{C9\text{-}C10}$, $\pi_{C1\text{-}C2} \rightarrow \pi^*_{C7\text{-}C8}$, and $\pi_{C9\text{-}C10} \rightarrow \pi^*_{C7\text{-}C8}$ donor–acceptor interactions.

The solvatochromism of dyes **2b**–**9b** was investigated in 28 solvents of different polarity. Table 2 shows the [E_T(dye)] values for each solvent, calculated from the λ_{max} values obtained from the UV–vis spectra, and also the corresponding E_T(30) values of betaine dye **1**. Figure 7 shows the plot of E_T(dye) as a function of E_T(30) for dye **8b**, which is representative for all dyes studied (see the Supporting Information), indicating the presence of two regions, one in less polar solvents and the other in more polar solvents. Starting with water, the most polar solvent studied, the E_T values for each dye decrease until solvents of intermediate polarities, after which this behavior changed; i.e., the E_T values increase with a further reduction in solvent polarity, with a reverse solvatochromism occurring. For dye **8b**, the solvatochromic band has a maximum at 572 nm [E_T(**8b**) = 50.0 kcal mol^{-1}] in cyclohexane, while, in DMSO, λ_{max} = 718 nm [E_T(**8b**) = 39.8 kcal mol^{-1}] is obtained. Thus, a reduction in the E_T(**8b**) value occurs with an increase in the polarity of the medium, leading to a bathochromic shift of $\Delta\lambda_{max}$ = +146 nm, which is characteristic for a positive solvatochromism.

DOI: 10.1021/acs.joc.5b00983
J. Org. Chem. 2015, 80, 7971–7983

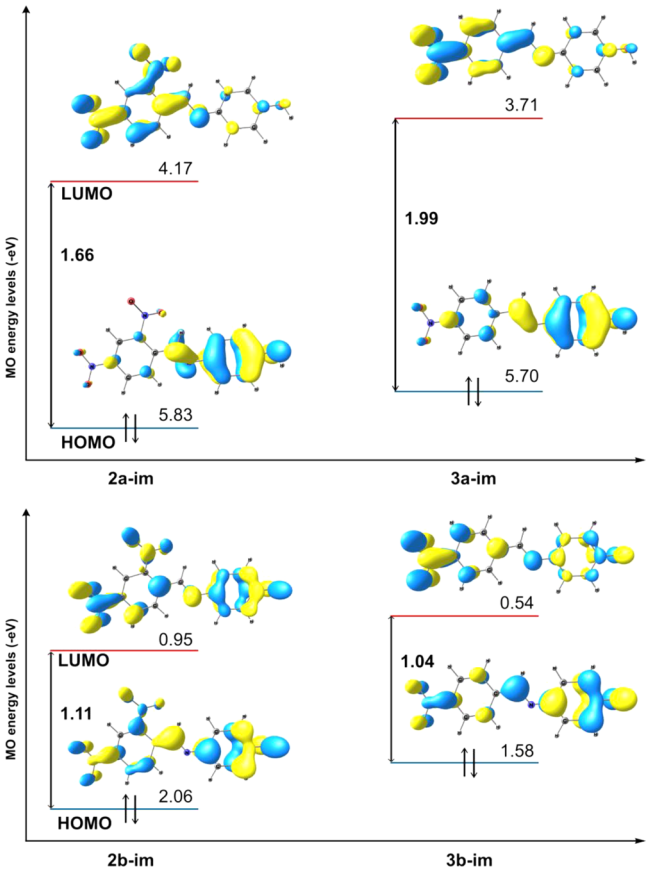

Figure 5. Contour plots and energies of the frontier orbitals (HOMO and LUMO) for compounds **2a-im**, **3a-im**, **2b-im**, and **3b-im**.

The region in the plot corresponding to DMSO as solvent is where the reversal in the solvatochromism starts to occur. Above this solvent polarity, a further increase in the solvent polarity leads to an increase in the E_T(**8b**) value, which is typical for a negative solvatochromism. The vis band of **8b** in water has a maximum at 496 nm [E_T(**8b**) = 57.6 kcal mol^{-1}], which, in comparison with the λ_{max} value in DMSO, corresponds to a strong hypsochromic band shift of $\Delta\lambda_{max}$ = −222 nm. The other dyes studied reveal a similar behavior, with a reversal in the solvatochromism occurring in DMA as solvent.

Table 3 lists the λ_{max} values for dyes **2b**−**9b** in the least polar, intermediate polar, and most polar solvent, as well as the $\Delta\lambda_{max}$ values for the bathochromic and hypsochromic band shifts corresponding to each dye. The data show that the compounds with two nitro groups in their molecular structure (**2b**, **4b**, **6b**, and **8b**) exhibit larger $\Delta\lambda_{max}$ values than their counterparts containing only one nitro group (**3b**, **5b**, **7b**, and **9b**). Of the compounds with two nitro groups, compound **8b** exhibits the highest $\Delta\lambda_{max}$ value, followed by dyes **2b**, **6b**, and **4b**. These results suggest that the positive inductive effect of the methyl groups in dye **8b** represents an important contribution to the charge transfer, while, for dyes **6b** and **4b**, the chloro and bromo substituents have positive mesomeric effects counterbalanced by the negative inductive effect due to their pronounced electronegativity. Concerning the dyes with only one nitro group, **7b** and **5b** exhibit lower $\Delta\lambda_{max}$ values in comparison with **3b**, which suggests that the electron-withdrawing effect of the halogens is responsible for the reduced probability of charge transfer from the phenolate to the nitrophenyl group in these dyes.

El Seoud et al.[28] proposed a methodology to evaluate the different factors that can contribute to the reverse solvatochromism of dyes. Thus, studies were performed for probes **2b**−**9b** in three solvents (of small, intermediate, and high polarity), in which the possibility of aggregation in the concentrations used in the spectrophotometric experiments or *cis-trans* isomerization (see the Supporting Information) was discarded.

Compounds **2b**−**9b** are salts, which can form, in principle, ion pairs in solution, especially in low polarity solvents. The formation of ion pairs would influence the absorption spectra of the dyes in these solvents. In order to verify this, UV−vis absorption spectra of the dye in toluene were collected in the presence of increasing concentrations of tetra-*n*-butylammonium iodide. It was verified that the addition of this salt up to 3.5 × 10^{-3} mol L^{-1} did not change the position of the maximum on the UV−vis spectra of **2b**−**9b** (see the Supporting Information). In another experiment, compound **6a** in toluene was deprotonated after the addition of potassium hydroxide (see the Supporting Information). The UV−vis spectrum was measured, and the solvatochromic band of **6b** has a maximum at 468 nm, which is very different from the value obtained if tetra-*n*-butylammonium hydroxide is used (λ_{max} = 526 nm). The results suggest an electrostatic interaction of potassium cation with the phenolate moiety of the dye. 18-Crown-6, a receptor highly selective for potassium ion, was added to the solution, and the UV−vis spectrum was made. The spectrum obtained is exactly the same as that measured in the presence of tetra-*n*-butylammonium hydroxide. The results showed that the solvatochromism observed is not influenced by the presence of tetra-*n*-butylammonium cation as a counteranion in the concentrations used in the experiment.

Therefore, the solvatochromism of the stilbenes should be interpreted in terms of the ability of the medium to stabilize the electronic ground and excited states of the dyes. According to Figure 8A, two resonance structures make a very important contribution to the resonance hybrid in compounds **2b**−**9b**, the quinonoid (less dipolar) and the benzenoid (more dipolar) forms. The resonance form that contributes mostly to the resonance hybrid is dependent on the solvent. Figure 8B represents schematically the reverse solvatochromism exhibited by dye **5b**, and this is representative of all of the other dyes studied herein. In less polar solvents, such as cyclohexane, the quinonoid form represents the most important contribution to the ground state. However, with a gradual increase in the solvent polarity, the difference between the energies for the ground and excited states is reduced, due to the fact that the solvent is less able to solvate the ground state of the dye, but more able to stabilize the more dipolar excited state. This explains the region of positive solvatochromism verified for these dyes in solvents with polarities between those of cyclohexane and DMA. In more polar solvents, such as water, the stabilization of the more dipolar benzenoid form is better in comparison with the less dipolar quinonoid form, and thus it makes a more important contribution under the conditions to the resonance hybrid, and, consequently, to the ground state of the dye. In this polarity range, an increase in the polarity of the medium leads to an increase in the difference, in terms of the energy, between the ground and the excited states, with negative solvatochromism being observed.

Multiparametric Studies on the Solvatochromism of 2b−**9b.** The Kamlet−Abboud−Taft[20,37−41] and Catalán[41−46] multiparameter equations were used in the analysis of the

DOI: 10.1021/acs.joc.5b00983
J. Org. Chem. 2015, 80, 7971−7983

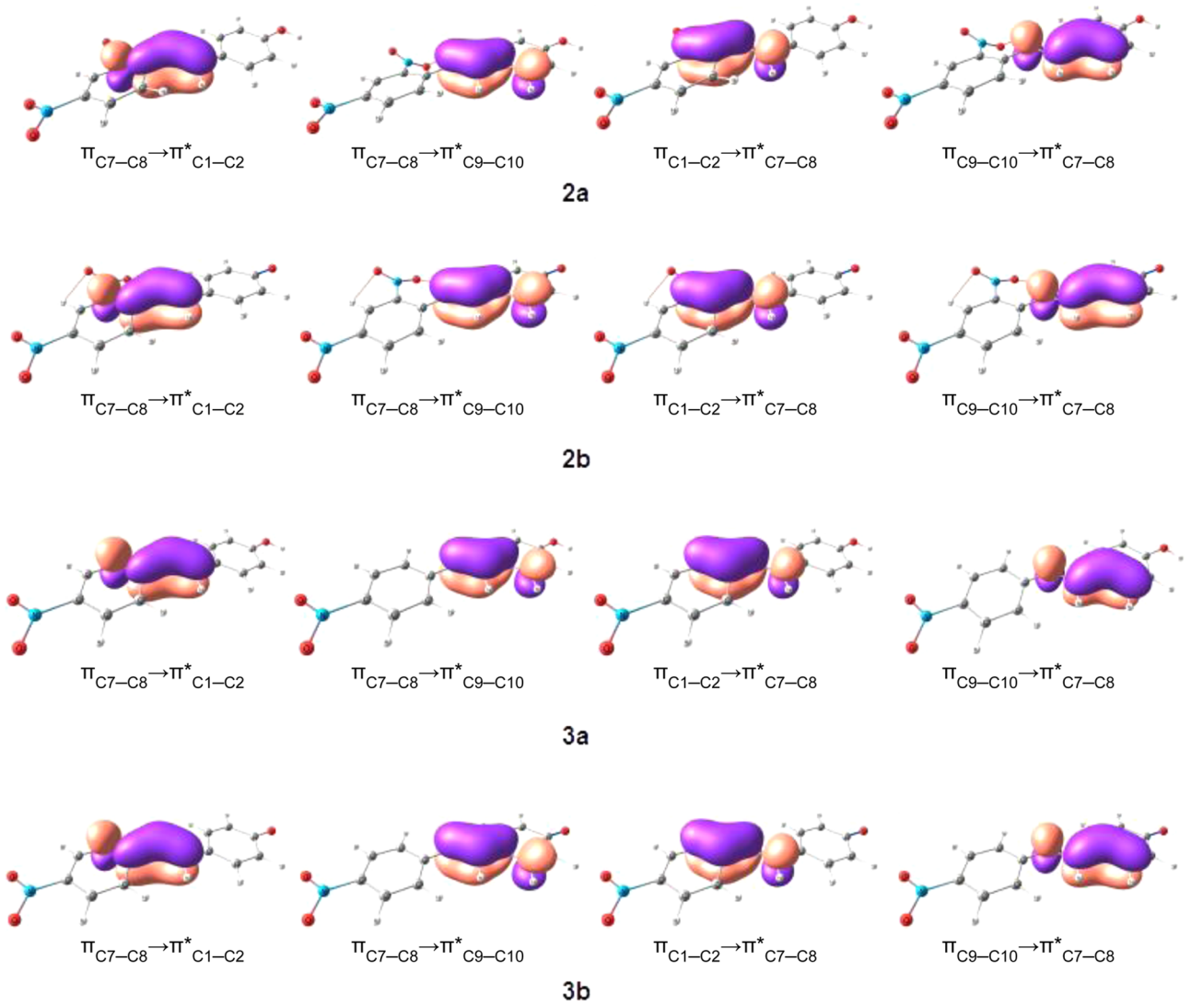

Figure 6. Plots for selected donor–acceptor interactions between NBOs of **2a**,**b** and **3a**,**b**.

experimental E_T(dye) values for compounds **2b**–**9b** in pure solvents. These approaches consider a linear correlation between the experimentally obtained spectrometric parameter, E_T(dye), and several solvent parameters according to eq 1. $E_T(\text{dye})_0$ represents the E_T(dye) value related to an inert solvent or the gas phase, and a, b, and c are coefficients that reflect the relative importance of the solvent parameters *A*, *B*, and *C*, respectively, in terms of E_T(dye).

$$E_T(\text{dye}) = E_T(\text{dye})_0 + aA + bB + cC + \ldots \quad (1)$$

The Kamlet–Abboud–Taft equation[37,38] requires the use of eq 2, where α, β, and π^* are parameters that represent the solvent hydrogen-bond donor (HBD) acidity, hydrogen-bond acceptor (HBA) basicity, and solvent dipolarity/polarizability, respectively, while δ is a polarizability correction term for the solvent. In the multiparameter equation developed by Catalán et al.,[45] eq 3 is used, where *SP* (solvent polarizability) and *SdP* (solvent dipolarity) are nonspecific and *SA* (solvent HBD acidity) and *SB* (solvent HBA basicity) are specific solvent parameters.

$$E_T(\text{dye}) = E_T(\text{dye})_0 + a\alpha + b\beta + s(\pi^* + d\delta) \quad (2)$$

$$E_T(\text{dye}) = E_T(\text{dye})_0 + aSA + bSB + cSP + dSdP \quad (3)$$

The contributions of the solvent properties to the E_T(dye) values determined for probes **2b**–**9b** were ascertained with the use of eqs 2 and 3. The data obtained from the multiple square correlation analysis are shown in Table 4, as well as Tables S2–S5, and S6 (Supporting Information). The use of eq 2 gives reasonable S.D. and *r* values; however, the b values are very large and the *s* values are very small for all dyes studied. These data are not consistent with the molecular structure of the probes, since they do not have hydrogen-bond donating groups to interact with HBA solvents. In addition, these compounds are expected to be considerably sensitive to the dipolarity/polarizability of the medium. The application of eq 3 to compounds **2b**–**9b** provides more coherent results: (a) the *r* values are >0.95 for all solvents studied; (b) the contribution of the HBA basicity of the solvent is small (small b coefficients); (c) the most important contributions were verified for the HBD acidity of the solvent (large a coefficients; for instance, for probe **2b** a/c = 16.37/12.62 = 1.30 and a/d = 16.37/8.64 = 1.89); and (d) the coefficients related to the polarizability and dipolarity of the medium represent important contributions to the solvatochromism exhibited by the dyes. The a/c ratio for the acidity and polarizability coefficients for probe **2b** is a/c = 16.37/12.62 = 1.30, while a comparison between the

DOI: 10.1021/acs.joc.5b00983
J. Org. Chem. 2015, 80, 7971–7983

Table 2. E_T(dye) Values for Compounds 2b−9b in 28 Pure Solvents at 25 °C and the E_T(30) Values in kcal mol^{-1}

solvent	E_T(30)[a]	E_T(2b)	E_T(3b)	E_T(4b)	E_T(5b)	E_T(6b)	E_T(7b)	E_T(8b)	E_T(9b)
water	63.1	61.4	66.8	62.7	67.4	63.0	67.7	57.6	63.0
ethane-1,2-diol	56.3	58.1	69.4	59.3	65.3	59.8	65.6	53.3	60.8
methanol	55.4	59.1	67.1	59.3	65.6	60.1	66.2	53.1	61.1
ethanol	51.9	55.4	62.7	55.8	63.0	56.5	63.5	49.0	57.4
propan-1-ol	50.7	54.1	61.6	55.0	62.4	55.4	62.4	48.1	56.7
benzyl alcohol	50.4	53.3	60.1	53.9	60.6	54.4	61.1	47.5	55.4
butan-1-ol	49.7	53.5	60.8	54.4	61.9	55.0	62.4	47.5	56.0
pentan-1-ol	49.1	53.1	60.8	54.1	61.6	54.6	62.2	46.9	55.8
propan-2-ol	48.4	51.4	59.1	52.7	60.3	52.7	60.6	45.1	55.5
octan-1-ol	48.1	52.4	59.8	53.5	61.1	53.9	61.4	47.5	55.8
decan-1-ol	47.7	52.7	60.8	53.9	61.6	54.4	62.2	47.5	55.8
butan-2-ol	47.1	50.0	57.9	52.0	59.6	52.0	59.8	44.0	52.6
acetonitrile	45.6	49.3	55.8	52.0	59.1	52.4	59.1	43.0	52.0
DMSO	45.1	42.7	50.0	47.6	54.4	48.0	54.1	39.8	45.0
2-methylpropan-2-ol	43.7	47.5	55.4	51.2	59.1	51.0	59.1	42.7	51.6
DMF	43.2	43.2	51.0	48.8	54.8	47.6	54.8	40.3	46.3
DMA	42.9	41.9	49.8	46.9	53.5	46.5	53.1	40.0	47.5
acetone	42.2	47.5	53.9	50.0	56.7	50.0	57.0	41.6	49.8
1,2-dichloroethane	41.3	49.8	57.0	51.2	59.1	51.8	59.3	43.4	54.1
dichloromethane	40.7	49.5	57.0	50.5	59.1	50.5	59.3	43.6	54.1
acetophenone	40.6	46.7	55.4	49.1	57.4	49.8	57.9	41.0	50.7
trichloromethane	39.1	50.5	57.9	51.4	59.3	52.4	60.1	45.7	55.2
ethyl acetate	38.1	48.8	55.8	50.5	58.3	50.5	58.3	42.7	52.6
THF	37.4	47.0	55.8	50.2	57.9	50.0	57.6	41.9	50.7
diethyl ether	34.5	50.5	58.8	52.6	60.1	52.0	60.1	45.0	54.8
toluene	33.9	53.1	61.1	54.1	61.4	54.4	62.2	48.3	57.9
n-hexane	31.0	56.5	63.5	55.8	64.1	57.9	65.3	50.0	59.1
cyclohexane	30.9	55.0	64.1	55.8	63.5	57.2	64.1	50.0	59.1

[a]Values obtained from the literature.[1]

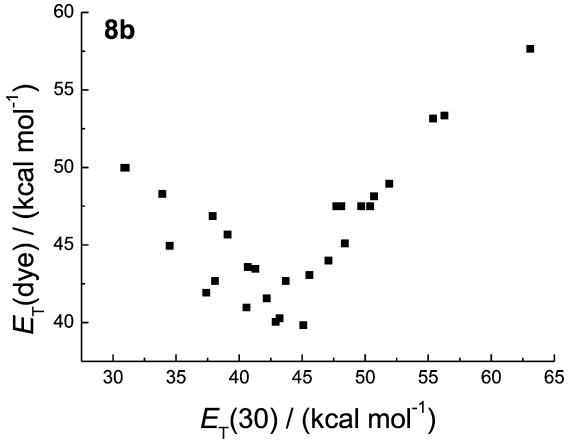

Figure 7. E_T(**8b**) values for 28 solvents as a function of Reichardt's E_T(30) parameter.

contribution of the polarizability and dipolarity terms gives the ratio c/d = 12.62/8.64 = 1.46. For compounds **2b**−**7b**, the contribution of the polarizability term is more important than the dipolarity term. However, for dyes **8b** and **9b**, which have methyl groups in their molecular structures, the dipolarity term has a larger contribution than the polarizability term.

Figure 9A shows plots of the experimentally obtained E_T(dye) values as a function of the E_T(dye) values calculated for dyes **4b** and **5b**, using the data from Table 4. Figure 9B shows the same plots using eq 3, but without the acidity term, verifying a decrease in the *r* value from 0.98 to 0.44 and from 0.97 to 0.51 for dyes **4b** and **5b**, respectively. The suppression of the basicity term in eq 3 has practically no influence on the *r* values (Figure 9C). Figure 9D shows the plots for the calculated data in which both the polarizability and dipolarity terms of eq 3 were suppressed. In this case, the *r* values decreased to 0.85 for dye **4b** and 0.76 for **5b**.

CONCLUSIONS

4-(Nitrostyryl)phenols **2a**−**9a** were synthesized and characterized, and their deprotonation in solution led to the formation of the corresponding phenolates (**2b**−**9b**). All compounds studied exhibited a reversal in solvatochromism. The change in the nature of the solvatochromism was verified, from positive in solvents of low polarity to negative in more polar solvents, in the region corresponding to DMA (E_T(30) = 42.9 kcal mol^{-1}) for dyes **2b**−**7b**. These results are, in general, similar to those obtained by Nandi et al.[23] for related dyes with an imino group as the conjugate bridge. For dyes **8b** and **9b**, the change observed from negative to positive solvatochromism occurs with DMSO (E_T(30) = 45.1 kcal mol^{-1}) as the solvent. Through a comparison between the dyes, it was verified that the phenolates with an additional nitro group in their molecular structure exhibit a more accentuated solvatochromism.

The solvatochromic behavior of the compounds is interpreted in terms of the interaction of the solvent with the electronic ground and excited states of the dyes, considering two resonance structures, i.e., quinonoid (less dipolar) and benzenoid (more dipolar) forms, whose contribution to the resonance hybrid is dependent on the solvent polarity. The Catalán multiparameter equation works very well for the fitting of the experimental data and shows that the dyes have, as

DOI: 10.1021/acs.joc.5b00983
J. Org. Chem. 2015, 80, 7971−7983

Table 3. Values of λ_{max} for Compounds 2b−9b in the Most Polar, Intermediate Polarity, and Least Polar Solvents, as Well as the $\Delta\lambda_{max}$ Values Obtained Considering the Regions of Positive and Negative Solvatochromism

dye	most polar solvent (water) λ_{max}/nm	intermediate polar solvent λ_{max}/nm	least polar solvent (cyclohexane) λ_{max}/nm	$\Delta\lambda_{max}{}^{a}$/nm	$\Delta\lambda_{max}{}^{b}$/nm
2b	466	682 (DMA)	520	+162	−216
3b	428	574 (DMA)	446	+128	−146
4b	456	610 (DMA)	512	+98	−154
5b	424	534 (DMA)	450	+84	−110
6b	454	614 (DMA)	500	+114	−160
7b	420	538 (DMA)	446	+92	−118
8b	496	718 (DMSO)	572	+146	−222
9b	454	636 (DMSO)	484	+152	−182

$^{a}\Delta\lambda_{max} = \lambda_{max}$ (intermediate solvent) − λ_{max} (least polar solvent). $^{b}\Delta\lambda_{max} = \lambda_{max}$ (water) − λ_{max} (intermediate solvent).

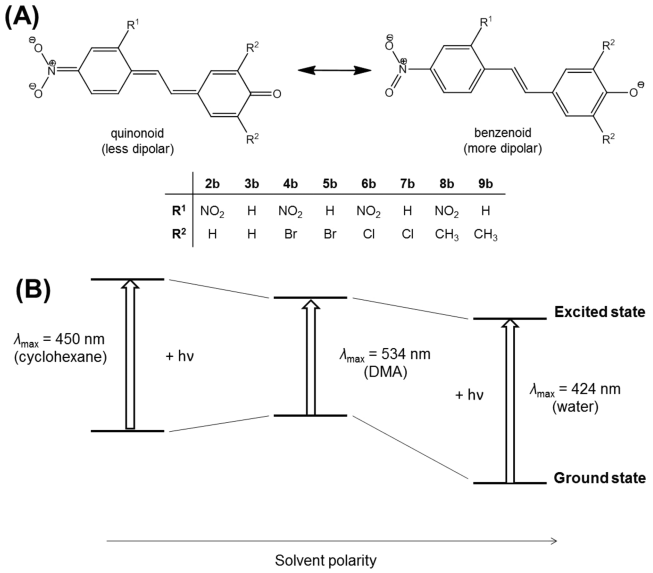

Figure 8. (A) Benzenoid and quinonoid resonance structures of compounds **2b−9b**. (B) Reverse solvatochromism exhibited by compound **5b**.

expected, poor sensitivity to the basicity of the medium and high sensitivity to the acidity of the medium, which can be understood in terms of the ability of HBD solvents to interact through hydrogen bonding with the phenolate moiety in the dyes. In addition, the polarizability and dipolarity of the medium make important contributions to the solvatochromism reported for these dyes.

In conclusion, the strong solvatochromic behavior of dyes **2b−9b** should motivate the synthesis of other related compounds aimed at not only understanding the reverse solvatochromism in these and other systems but also obtaining increasingly more effective solvatochromic systems. The strong solvatochromism exhibited by this class of compounds is of interest in relation to the design of systems aimed at the investigation of their perichromic properties, such as in the investigation of the polarity of solvent mixtures, cyclodextrins, and surfactants in water, and also in the development of optical devices, which can be used for the detection of analytes and in organic electronics.

EXPERIMENTAL SECTION

Materials and Methods. All solvents were HPLC grade and were purified following the methodology described in the literature.[47,48] Deionized water was used in all measurements, and it was boiled and bubbled with nitrogen and kept in a nitrogen atmosphere to avoid the presence of carbon dioxide.

The melting points were uncorrected. IR spectra were obtained with KBr pellets. The NMR spectra were recorded in $CDCl_3$, DMSO-d_6, or acetone-d_6 with 200 and 400 MHz spectrometers. Chemical shifts were recorded in ppm with the solvent resonance as the internal standard, and data are reported as follows: chemical shift, multiplicity (*s* = singlet, *d* = doublet, *t* = triplet, *dd* = double doublet), coupling constants (Hz), and integration. High-resolution mass spectra were obtained with an electrospray ionization-quadrupole time-of-flight mass spectrometer (HR ESI-MS QTOF).

Synthesis of the Compounds. 2,4-Dinitrotoluene (**10**) was prepared according to the procedure described in the literature,[47] the melting point obtained being 69−70 °C (literature melting point of 70 °C).[47]

3,5-Dibromo-4-hydroxybenzaldehyde (**11**) was obtained based on the methodology described by Mahajan and co-workers[49] with some modifications: 60 mL of water was heated to 40 °C and 4-hydroxybenzaldehyde (6.00 g, 49.1 mmol), potassium bromide (17.53 g, 147.3 mmol), 4-toluenesulfonic acid (16.90 g, 98.2 mmol), and finally *N*-bromosuccinimide (17.48 g, 98.2 mmol) were added and reacted for 2 h. The compound was filtered off, washed with a solution of sodium metabisulfite ($Na_2S_2O_5$, 10%), and recrystallized twice from a mixture of water/ethanol. The product is a colorless solid (8.25 g, 60% yield) with a melting point of 181 °C.

Table 4. Regression Coefficients a, b, c, and d Obtained from Catalán Multiparametric Analysis, Significance (*F*), Correlation Coefficient (*r*), and Standard Deviation (S.D.) Obtained from the Treatment of E_T(dye) Values for Compounds 2b−9b in 28 Solvents

dye	constant	*A*	b	c	d	*F*	*r*	S.D.
2b	64.94 ± 2.98	16.37 ± 1.18	−4.33 ± 1.00	−12.62 ± 4.13	−8.64 ± 1.17	$<3.30 \times 10^{-12}$	0.96	1.46
3b	71.46 ± 3.46	15.48 ± 1.29	−3.33 ± 1.10	−10.54 ± 4.52	−9.79 ± 1.28	$<5.14 \times 10^{-11}$	0.95	1.60
4b	62.78 ± 1.62	13.12 ± 0.64	−3.20 ± 0.54	−10.19 ± 2.24	−5.24 ± 0.63	$<1.66 \times 10^{-15}$	0.98	0.80
5b	70.90 ± 1.90	11.37 ± 0.75	−2.70 ± 0.64	−10.14 ± 2.62	−6.40 ± 0.74	$<3.57 \times 10^{-13}$	0.97	0.93
6b	64.02 ± 2.00	13.90 ± 0.79	−3.86 ± 0.67	−10.11 ± 2.76	−6.41 ± 0.78	$<3.15 \times 10^{-14}$	0.97	0.98
7b	71.67 ± 2.10	12.09 ± 0.83	−3.12 ± 0.70	−9.92 ± 2.91	−7.21 ± 0.82	$<7.22 \times 10^{-13}$	0.96	1.03
8b	54.60 ± 1.79	16.30 ± 0.70	−4.09 ± 0.60	−6.53 ± 2.47	−7.73 ± 0.70	$<1.11 \times 10^{-16}$	0.98	0.88
9b	66.65 ± 3.04	14.24 ± 1.20	−4.65 ± 1.02	−9.14 ± 4.21	−9.15 ± 1.19	$<3.47 \times 10^{-11}$	0.95	1.49

DOI: 10.1021/acs.joc.5b00983
J. Org. Chem. 2015, 80, 7971−7983

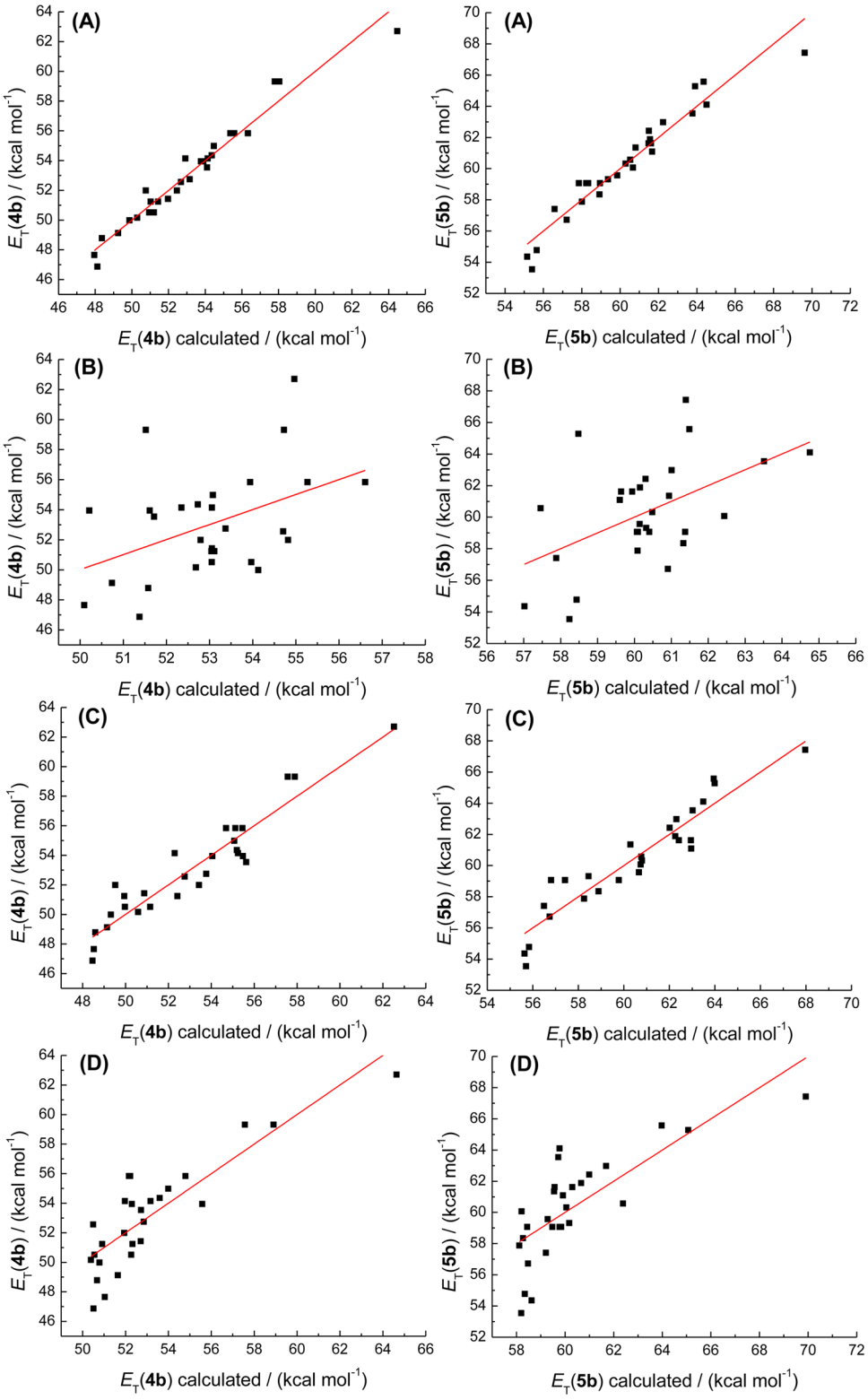

Figure 9. Relationship between experimental and calculated E_T values for the compounds **4b** and **5b** with all terms (A), without the acidity term (B), without the basicity term (C), and without polarizability and dipolarity terms (D).

3,5-Dichloro-4-hydroxybenzaldehyde (**12**) was obtained according to the procedure described in the literature[49] with a melting point of 154−157 °C.

3,5-Dimethyl-4-hydroxybenzaldehyde (**13**) was synthesized according to the literature,[50] but the purification was performed on a chromatographic column with *n*-hexane/ethyl acetate (7:3 v/v). The product has a melting point of 112−114 °C.

4-Nitrobenzyl-triphenylphosphonium bromide (**14**) was prepared based on the methodology described by Sá and co-workers.[36] 1-(Bromomethyl)-4-nitrobenzene (0.22 g, 1 mmol) and triphenylphosphane (0.27 g, 1 mmol) were added to 3 mL of acetonitrile, and the solution was stirred at 25 °C for 24 h. The product is colorless (0.38 g, 80% yield) and has a melting point of 273−274 °C.

DOI: 10.1021/acs.joc.5b00983
J. Org. Chem. 2015, 80, 7971−7983

Table 5. Crystal Data of Compounds 4a, 6a, and 8a

	4a	6a	8a
CCDC no.	1062279	1062280	1062281
empirical formula	$C_{14}H_8Br_2N_2O_5$	$C_{17}H_{14}Cl_2N_2O_6$	$C_{16}H_{14}N_2O_5$
formula weight	444.04	413.20	314.29
temperature/K	173(2)	173(2)	293(2)
wavelength/Å	0.71073	0.71073	0.71073
crystal system	monoclinic	monoclinic	triclinic
space group	$P2_1/c$	$P2_1/c$	$P\bar{1}$
a/Å	15.3818(4)	17.2796(4)	6.9348(2)
α/deg	90	90	81.896(1)
b/Å	6.9603(2)	7.1834(2)	7.8591(2)
β/deg	119.2930(10)	94.5170(10)	77.827(1)
c/Å	15.6549(4)	14.5636(3)	15.3115(3)
γ/deg	90	90	64.116(1)
volume/Å^3	1461.73(7)	1802.11(8)	732.76(3)
Z	4	4	2
density (calculated)/g cm^{-3}	2.018	1.523	1.424
absorption coefficient/mm^{-1}	5.574	0.398	0.108
F(000)	864	848	328
crystal size/mm^3	0.26 × 0.24 × 0.02	0.30 × 0.18 × 0.06	0.38 × 0.28 × 0.08
θ range for data collection/deg	2.60−34.09	2.36−33.10	2.73−32.38
index ranges	$-22 \le h \le 24$	$-25 \le h \le 26$	$-10 \le h \le 10$
	$-9 \le k \le 10$	$-7 \le k \le 11$	$-11 \le k \le 9$
	$-24 \le l \le 24$	$-22 \le l \le 22$	$-23 \le l \le 23$
reflections collected	16499	26613	11136
independent reflections	5939 [R(int) = 0.0212]	6823 [R(int) = 0.0157]	5218 [R(int) = 0.0151]
absorption correction	semiempirical from equivalents		
max and min transmission	0.8967 and 0.3251	0.9765 and 0.8899	0.9914 and 0.9602
refinement method	full-matrix least-squares on F^2		
data/restraints/parameters	5939/0/208	6823/0/256	5218/0/209
goodness-of-fit on F^2	1.019	1.043	1.068
final R indices [$I > 2\sigma(I)$]	R_1 = 0.0279,	R_1 = 0.0341	R_1 = 0.0561
	wR_2 = 0.0624	wR_2 = 0.0920	wR_2 = 0.1736
R indices (all data)	R_1 = 0.0448	R_1 = 0.0420	R_1 = 0.0715
	wR_2 = 0.0682	wR_2 = 0.0989	wR_2 = 0.1918
largest diff. peak and hole/e Å^{-3}	1.020 and −0.729	0.442 and −0.387	0.472 and −0.291

*(E)-4-(2,4-Dinitrostyryl)phenol (**2a**).* This compound was prepared based on the methodology described by Saravanan and Srinivasan[34] with some modifications: 2,4-dinitrotoluene (1.00 g, 5.5 mmol), 4-hydroxybenzaldehyde (0.67 g, 5.5 mmol), and pyrrolidine (360 μL, 4.4 mmol) were refluxed at 90 °C for 4 h. The compound was purified by column chromatography using methanol/trichloromethane (1:1 v/v) as the eluent and then by recrystallization from methanol. The product is an orange solid (0.50 g, 32% yield) with a melting point of 177−179 °C. IR (KBr, $\bar{\nu}_{max}$/cm^{-1}): 3408 (O−H), 3073 (=C−H), 1587, 1513, and 1440 (C=C), 1334 (N=O). ^{1}H NMR (400 MHz, DMSO-d_6) δ/ppm: 9.95 (1H, *s*), 8.70 (1H, *d*, *J* = 2.0 Hz), 8.43 (1H, *dd*, *J* = 2.0 Hz and *J* = 8.0 Hz), 8.21 (1H, *d*, *J* = 8.0 Hz), 7.54 (1H, *d*, *J* = 16.0 Hz), 7.51 (2H, *d*, *J* = 8.0 Hz), 7.27 (1H, *d*, *J* = 16.0 Hz), 6.81 (2H, *d*, *J* = 8.0 Hz).

*(E)-4-(4-Nitrostyryl)phenol (**3a**).* This compound was synthesized according to the literature[51] with a melting point of 204−206 °C. IR (KBr, $\bar{\nu}_{max}$/cm^{-1}): 3418 (O−H), 1585, 1501, and 1438 (C=C), 1338 (N=O). ^{1}H NMR (400 MHz, DMSO-d_6) δ/ppm: 9.70 (1H, *s*), 8.18 (2H, *d*, *J* = 8.0 Hz), 7.77 (2H, *d*, *J* = 8.0 Hz), 7.50 (2H, *d*, *J* = 8.0 Hz), 7.42 (1H, *d*, *J* = 16.0 Hz), 7.16 (1H, *d*, *J* = 16.0 Hz), 6.80 (2H, *d*, *J* = 8.0 Hz).

*(E)-2,6-Dibromo-4-(2,4-dinitrostyryl)phenol (**4a**).* 2,4-Dinitrotoluene (0.27 g, 1.5 mmol), 3,5-dibromo-4-hydroxybenzaldehyde (0.41 g, 1.5 mmol), and pyrrolidine (98 μL, 1.2 mmol) were refluxed at 80−85 °C for 6 h. Purification was performed by column chromatography, eluting with trichloromethane/*n*-hexane (9:1 v/v). A yellow solid was obtained (0.27 g, 41% yield) with a melting point of 273−275 °C; IR (KBr, $\bar{\nu}_{max}$/cm^{-1}): 3408 (O−H), 3098 (=C−H), 1593, 1521, and 1475 (C=C), 1346 (C=O); ^{1}H NMR (400 MHz, DMSO-d_6) δ/ppm: 10.39 (1H, *s*), 8.71 (1H, *d*, *J* = 2.0 Hz,), 8.51 (1H, *dd*, *J* = 2.0 Hz and *J* = 9.0 Hz), 8.14 (1H, *d*, *J* = 9.0 Hz), 7.91 (2H, *s*), 7.46 (2H, *s*); HRMS (ESI/TOF-Q) *m*/*z*: [M]$^-$ Calcd for $C_{14}H_7N_2O_5Br_2$ 440.8716; Found 440.8712.

*(E)-2,6-Dibromo-4-(4-nitrostyryl)phenol (**5a**).* *p*-Nitrotoluene (0.50 g, 3.6 mmol), 3,5-dibromo-4-hydroxybenzaldehyde (1.02 g, 3.6 mmol), and pyrrolidine (750 μL, 9.1 mmol) were refluxed at 70−75 °C for 72 h. In the purification, column chromatography was used, eluting with *n*-hexane/ethyl acetate (1:1 v/v). A yellow solid (0.39 g, 27% yield) was obtained with a melting point of 235−237 °C; IR (KBr, $\bar{\nu}_{max}$/cm^{-1}): 3467 (O−H), 3067 (=C−H), 1595, 1513, and 1472 (C=C), 1336 (C=O); ^{1}H NMR (400 MHz, DMSO-d_6) δ/ppm: 10.24 (1H, *s*), 8.22 (2H, *d*, *J* = 8.0 Hz), 7.88 (2H, *s*), 7.78 (2H, *d*, *J* = 8.0 Hz), 7.39 (2H, *s*); HRMS (ESI/TOF-Q) *m*/*z*: [M]$^-$ Calcd for $C_{14}H_8NO_3Br_2$ 395.8865; Found 395.8867.

*(E)-2,6-Dichloro-4-(2,4-dinitrostyryl)phenol (**6a**).* 2,4-Dinitrotoluene (1.00 g, 5.5 mmol), 3,5-dichloro-4-hydroxybenzaldehyde (1.04 g, 5.5 mmol), and pyrrolidine (360 μL, 4.4 mmol) were refluxed at 80−85 °C for 10 h. Chromatographic columns were used in the purification, eluting with *n*-hexane/ethyl acetate (7:3 v/v). A yellow solid (0.66 g, 34% yield) was obtained with a melting point of 249−251 °C; IR (KBr, $\bar{\nu}_{max}$/cm^{-1}): 3440 (O−H), 3101 (=C−H), 1594, 1522, and 1490 (C=C), 1349 (C=O); ^{1}H NMR (200 MHz, acetone-d_6) δ/ppm: 8.78 (1H, *d*, *J* = 2.0 Hz), 8.56 (1H, *dd*, *J* = 2.0 Hz and *J* = 9.0 Hz), 8.26 (1H, *d*, *J* = 9.0 Hz), 7.72 (2H, *s*), 7.61 (1H, *d*, *J* = 16.0 Hz), 7.47 (1H, *d*, *J* = 16.0 Hz); HRMS

DOI: 10.1021/acs.joc.5b00983
J. Org. Chem. 2015, 80, 7971−7983

(ESI/TOF-Q) *m*/*z*: $[M]^-$ Calcd for $C_{14}H_7N_2O_5Cl_2$ 352.9727; Found 352.9729.

*(E)-2,6-Dichloro-4-(4-nitrostyryl)phenol (**7a**).* 4-Nitrotoluene (0.42 g, 3.1 mmol), 3,5-dichloro-4-hydroxybenzaldehyde (0.59 g, 3.1 mmol), and pyrrolidine (625 μL, 7,6 mmol) were refluxed at 70−75 °C for 72 h. Purification was performed using column chromatography with the eluent *n*-hexane/ethyl acetate (7:3 v/v). A yellow solid (0.22 g, 23% yield) was obtained with a melting point of 169−171 °C; IR (KBr, $\bar{\nu}_{max}/cm^{-1}$): 3442 (O−H), 1591, 1513, and 1497 (C═C), 1348 (C═O); ^{1}H NMR (400 MHz, acetone-d_6) δ/ppm: 8.24 (2H, *d*, *J* = 8.0 Hz), 7.84 (2H, *d*, *J* = 8.0 Hz), 7.68 (2H, *s*), 7.40 (2H, *s*); ^{13}C NMR (50 MHz, acetone-d_6) δ/ppm: 150.7, 148.4, 145.4, 132.3, 131.9, 131.8, 128.6, 128.5, 128.1, 125.4, 123.8; HRMS (ESI/TOF-Q) *m*/*z*: $[M]^-$ Calcd for $C_{14}H_8NO_3Cl_2$ 307.98757; Found 307.98755.

*(E)-2,6-Dimethyl-4-(2,4-dinitrostyryl)phenol (**8a**).* 2,4-Dinitrotoluene (0.18 g, 1 mmol), 3,5-dimethyl-4-hydroxybenzaldehyde (0.15 g, 1 mmol), and pyrrolidine (65 μL, 0.8 mmol) were placed in a glass tube designed for use in a microwave oven. The reaction was irradiated by microwave for 25 min at a temperature of 80 °C using 100 W of power and pressure of 50 psi. The purification was performed by column chromatography with *n*-hexane/ethyl acetate (1:1 v/v) as the eluent and subsequent recrystallization from acetone. An orange solid (0.16 g, 51% yield) was obtained with a melting point of: 235−237 °C; IR (KBr, $\bar{\nu}_{max}/cm^{-1}$): 3524 (O−H), 3088 (═C−H), 2921 and 2851 (−C−H), 1585, 1524, and 1493 (C═C), 1348 (N═O); ^{1}H NMR (400 MHz, acetone-d_6) δ/ppm: 8.72 (1H, *d*, *J* = 2.0 Hz), 8.46 (1H, *dd*, *J* = 2.0 Hz and *J* = 9.0 Hz), 8.25 (1H, *d*, *J* = 9.0 Hz), 7.80 (1H, *s*), 7.49 (1H, *d*, *J* = 16.0 Hz), 7.41 (1H, *d*, *J* = 16.0 Hz), 7.32 (2H, *s*), 2.26 (6H, *s*); HRMS (ESI/TOF-Q) *m*/*z*: $[M]^-$ Calcd for $C_{16}H_{13}N_2O_5$ 313.0819; Found 313.0822.

*(E)-2,6-Dimethyl-4-(4-nitrostyryl)phenol (**9a**).* 4-Nitrobenzyl-triphenylphosphonium bromide (0.48 g, 1 mmol), 3,5-dimethyl-4-hydroxybenzaldehyde (0.15 g, 1 mmol), and $NaHCO_3$ (0.42 g, 5 mmol) were mixed with 5 mL of H_2O and 4 mL of DMSO, and the reaction mixture was stirred at 25 °C for 120 h. The reaction was quenched with aqueous HCl (1 mol L^{-1}), the aqueous solution was extracted three times with CH_2Cl_2, and the organic phase was washed twice with H_2O, dried with $MgSO_4$, and filtered under reduced pressure. The compound was purified by column chromatography using *n*-hexane/ethyl acetate (65:35 v/v) as eluent and then by recrystallization from propan-2-ol. A yellow solid (0.11 g, 40% yield) was obtained with a melting point of 138−139 °C; IR (KBr, $\bar{\nu}_{max}/cm^{-1}$): 3443 (O−H), 2919 (−C−H), 1589, 1513, and 1489 (C═C), 1338 (N═O); ^{1}H NMR (200 MHz, acetone-d_6) δ/ppm: 8.19 (2H, *d*, *J* = 9.0 Hz), 7.77 (2H, *d*, *J* = 9.0 Hz), 7.60 (1H, *s*), 7.37 (1H, *d*, *J* = 16.7 Hz), 7.27 (2H, *s*), 7.16 (1H, *d*, *J* = 16.7 Hz), 2.25 (6H, *s*); HRMS (ESI/TOF-Q) *m*/*z*: $[M]^-$ Calcd for $C_{16}H_{14}NO_3$ 268.0968; Found 268.0966.

UV−vis Measurements. The following procedure was typical for all measurements performed. A 5.0×10^{-3}-1.0×10^{-2} mol L^{-1} stock solution of each compound was prepared in acetone. From this stock solution, 4−16 μL were transferred to twenty-eight 5 mL volumetric flasks. After evaporation of the acetone, the probe was dissolved in the pure solvent, resulting in a solution presenting a final dye concentration of 2.0×10^{-5} to 4.0×10^{-5} mol L^{-1}. In order to generate the deprotonated compounds, 20 μL of an methanolic 0.1 mol L^{-1} tetra-*n*-butylammonium hydroxide solution was added to each flask. The addition of this very small amount of methanol did not change the position of the UV−vis band of the dye. The bulky tetra-*n*-butylammonium ion has no influence on the UV−vis spectrum of the anionic dye. The UV−vis spectra were recorded at 25 °C, using a 1 cm square cuvette. The maxima of the UV−vis spectra were calculated from the first derivative of the absorption spectrum, with a precision of ±0.5 nm, and the reproducibility of the λ_{max} values was verified through the determination of five spectra for each dye in each pure solvent. The λ_{max} values thus obtained were transformed into E_T(dye) values, according to the expression $E_T(dye) = 28590/\lambda_{max}$,[1,5] given in kcal mol^{-1} with a precision of ±0.1 kcal mol^{-1}.

Computational Details. Geometry optimizations, stretching frequency calculations, and the analysis of CMOs (canonical molecular orbitals) were performed at the DFT level (BP86[52,53]-D3[54]/def2-TZVP).[55] NBO (natural bond orbital) analysis was performed at the BP86/def2-SVP[55] level. All calculations were performed using the ORCA[56] package. NBO analysis was performed using NBO[57] 5.9 as implemented in GAMESS-US.[58]

Single-Crystal X-ray Structure Determinations. X-ray diffraction data were recorded on a Bruker APX-II DUO diffractometer equipped with an APEX II CCD area detector using graphite-monochromated Mo Kα (λ = 0.71073 Å). The temperature was set at 173 K for compound **4a** and **6a** and 293 K for **8a**. The frames were recorded by ω and ϕ scans using APEX2,[59] and the integration procedure was performed using the SAINT and SADABS programs.[59] The structures were solved and refined with SHELXS97 and SHELXL2013 software programs,[60] respectively. All non-hydrogen atoms were refined anisotropically. Hydrogen atoms attached to C atoms were placed at their idealized positions using standard geometric criteria. Hydrogen atoms of the hydroxyl groups were located from the Fourier difference map and treated with riding model approximation. The ORTEP plot was obtained with PLATON software.[61] For compound **6a**, one atom of oxygen of the nitro group at position 2 of the acceptor aromatic ring is disordered over two alternative positions, with a refined site occupation of 0.558(5) and 0.442(5). Further crystallographic information is given in Table 5. Full tables containing the crystallographic data (except structural factors) have been deposited at the Cambridge Structural Database, as supplementary publications nos. 1062279−1062281. Copies of the data can be obtained free of charge at www.ccdc.cam.ac.uk.

Calculation Methods. The multiparametric analysis was performed from nonlinear regressions using ORIGIN 8.5 software.

■ ASSOCIATED CONTENT

Supporting Information

The Supporting Information is available free of charge on the ACS Publications website at DOI: 10.1021/acs.joc.5b00983.

IR, HRMS, ^{1}H, and ^{13}C NMR data for compounds **2a−9a**; experiments used to discard aggregation of the compounds; UV−vis spectra of **2b−9b** at 25 and 50 °C; "polarity" parameters for the pure solvents; tables containing the correlation coefficients obtained from the multiparametric analyses; correlation between experimental and calculated E_T values for dyes **2b−9b**; tables reporting bond lengths, angles, torsion angles, and hydrogen bonds for compounds **2a−9a**; and tables showing data related to the NBO analysis for protonated and deprotonated analogues and atom coordinates of optimized structures for the compounds (PDF)

Tables reporting bond lengths, angles, torsion angles, and hydrogen bonds for compound **4a** (PDF)

Tables reporting bond lengths, angles, torsion angles, and hydrogen bonds for compound **6a** (PDF)

Tables reporting bond lengths, angles, torsion angles, and hydrogen bonds for compound **8a** (PDF)

X-ray crystallographic data for compound **4a** (CIF)

X-ray crystallographic data for compound **6a** (CIF)

X-ray crystallographic data for compound **8a** (CIF)

■ AUTHOR INFORMATION

Corresponding Author

*E-mail: vanderlei.machado@ufsc.br.

Notes

The authors declare no competing financial interest.

■ ACKNOWLEDGMENTS

The financial support of the Brazilian Conselho Nacional de Desenvolvimento Científico e Tecnológico (CNPq), Coordenação

DOI: 10.1021/acs.joc.5b00983
J. Org. Chem. 2015, 80, 7971−7983

de Aperfeiçoamento de Pessoal de Nível Superior (CAPES), Laboratório Central de Biologia Molecular (CEBIME/UFSC), FINEP and UFSC is gratefully acknowledged. We thank also Professor Marcus M. Sá for laboratory facilities.

REFERENCES

(1) Reichardt, C.; Welton, T. *Solvents and Solvent Effects in Organic Chemistry*, 4th ed.; Wiley-VCH: Weinheim, 2011.
(2) Suppan, P.; Ghoneim, N. P. *Solvatochromism*; Royal Society of Chemistry: Cambridge, U.K., 1997.
(3) Bagno, A. *J. Phys. Org. Chem.* **2002**, *15*, 790.
(4) El Seoud, O. A. *Pure Appl. Chem.* **2009**, *81*, 697.
(5) Reichardt, C. *Chem. Rev.* **1994**, *94*, 2319.
(6) Katritzky, A. R.; Fara, D. C.; Yang, H.; Tämm, K.; Tamm, T.; Karelson, M. *Chem. Rev.* **2004**, *104*, 175.
(7) Reichardt, C. *Pure Appl. Chem.* **2004**, *76*, 1903.
(8) Reichardt, C. *Pure Appl. Chem.* **2008**, *80*, 1415.
(9) Machado, V. G.; Stock, R. I.; Reichardt, C. *Chem. Rev.* **2014**, *114*, 10429.
(10) Niedbalska, M.; Gruda, I. *Can. J. Chem.* **1990**, *68*, 691.
(11) Combellas, C.; Suba, C.; Thièbault, A. *Tetrahedron Lett.* **1992**, *33*, 5741.
(12) Catalán, J.; Mena, E.; Meutermans, W.; Elguero, J. *J. Phys. Chem.* **1992**, *96*, 3615.
(13) Abdel-Halim, S. T. *J. Chem. Soc., Faraday Trans.* **1993**, *89*, 55.
(14) Machado, C.; de Graça Nascimento, M.; Rezende, M. C. *J. Chem. Soc., Perkin Trans. 2* **1994**, 2539.
(15) da Silva, L.; Machado, C.; Rezende, M. C. *J. Chem. Soc., Perkin Trans. 2* **1995**, 483.
(16) Gonzalez, D.; Neilands, O.; Rezende, M. C. *J. Chem. Soc., Perkin Trans. 2* **1999**, 713.
(17) da Silva, D. C.; Ricken, I.; do R. Silva, M. A.; Machado, V. G. *J. Phys. Org. Chem.* **2002**, *15*, 420.
(18) Diemer, V.; Chaumeil, H.; Defoin, A.; Jacques, P.; Carré, C. *Tetrahedron Lett.* **2005**, *46*, 4737.
(19) Cavalli, V.; da Silva, D.; Machado, C.; Machado, V. G.; Soldi, V. *J. Fluoresc.* **2006**, *16*, 77.
(20) Martins, C. T.; Lima, M. S.; El Seoud, O. A. *J. Org. Chem.* **2006**, *71*, 9068.
(21) Domínguez, M.; Rezende, M. C. *J. Phys. Org. Chem.* **2010**, *23*, 156.
(22) Ay, E.; Chaumeil, H.; Barsella, A. *Tetrahedron* **2012**, *68*, 628.
(23) Nandi, L. G.; Facin, F.; Marini, V. G.; Zimmermann, L. M.; Giusti, L. A.; da Silva, R.; Caramori, G. F.; Machado, V. G. *J. Org. Chem.* **2012**, *77*, 10668.
(24) Benson, H. G.; Murrell, J. N. *J. Chem. Soc., Faraday Trans. 2* **1972**, *68*, 137.
(25) Mishra, B. K.; Kuanar, M.; Mishra, A.; Behera, G. B. *Bull. Chem. Soc. Jpn.* **1996**, *69*, 2581.
(26) Aliaga, C.; Galdames, J. S.; Rezende, M. C. *J. Chem. Soc., Perkin Trans. 2* **1997**, 1055.
(27) Panigrahi, M.; Dash, S.; Patel, S.; Behera, P. K.; Mishra, B. K. *Spectrochim. Acta, Part A* **2007**, *68*, 757.
(28) Martins, C. T.; Lima, M. S.; Bastos, E. L.; El Seoud, O. A. *Eur. J. Org. Chem.* **2008**, *2008*, 1165.
(29) Murugan, N. A.; Kongsted, J.; Rinkevicius, Z.; Ågren, H. *Phys. Chem. Chem. Phys.* **2011**, *13*, 1290.
(30) Tsukada, M.; Mineo, Y.; Itoh, K. *J. Phys. Chem.* **1989**, *93*, 7989.
(31) Hisamoto, H.; Tohma, H.; Yamada, T.; Yamauchi, K.-I.; Siswanta, D.; Yoshioka, N.; Suzuki, K. *Anal. Chim. Acta* **1998**, *373*, 271.
(32) Rezende, M. C. *J. Braz. Chem. Soc.* **1997**, *8*, 631.
(33) de Melo, C. E. A.; Nandi, L. G.; Domínguez, M.; Rezende, M. C.; Machado, V. G. *J. Phys. Org. Chem.* **2015**, *28*, 250.
(34) Saravanan, S.; Srinivasan, P. C. *Synth. Commun.* **2001**, *31*, 823.
(35) Likhtenshtein, G. *Stilbenes: Applications in Chemistry, Life Sciences and Materials Science*; Wiley-VCH: Weinheim, 2010.
(36) Meier, L.; Ferreira, M.; Sá, M. M. *Heteroat. Chem.* **2012**, *23*, 179.
(37) Kamlet, M. J.; Abboud, J. -L. M.; Abraham, M. H.; Taft, R. W. *J. Org. Chem.* **1983**, *48*, 2877.
(38) Marcus, Y. *Chem. Soc. Rev.* **1993**, *22*, 409.
(39) Trišović, N.; Valentić, N.; Uščumlić, G. *Chem. Cent. J.* **2011**, *5*, 62.
(40) El-Sayed, M.; Müller, H.; Rheinwald, G.; Lang, H.; Spange, S. *Chem. Mater.* **2003**, *15*, 746.
(41) Jayabharathi, J.; Thanikachalam, V.; Devi, K. B.; Perumal, M. V. *J. Fluoresc.* **2012**, *22*, 737.
(42) Catalán, J.; López, V.; Pérez, P.; Martin-Villamil, R.; Rodríguez, J.-G. *Liebigs Ann.* **1995**, *1995*, 241.
(43) Catalán, J.; López, V.; Pérez, P. *Liebigs Ann.* **1995**, *1995*, 793.
(44) Catalán, J.; Díaz, C.; López, V.; Pérez, P.; De Paz, J.-L. G.; Rodríguez, J. G. *Liebigs Ann.* **1996**, *1996*, 1785.
(45) Catalán, J. *J. Phys. Chem. B* **2009**, *113*, 5951.
(46) Catalán, J. *Dyes Pigm.* **2012**, *95*, 180.
(47) Vogel, A. I.; Tatchell, A. R.; Furniss, B. S.; Hannaford, A. J.; Smith, P. W. G. *Vogel's Textbook of Practical Organic Chemistry*, 5th ed.; Longman Group UK Limited: London, 1996.
(48) Williams, D. B. G.; Lawton, M. *J. Org. Chem.* **2010**, *75*, 8351.
(49) Mahajan, T.; Kumar, L.; Dwivedi, K.; Agarwal, D. D. *Ind. Eng. Chem. Res.* **2012**, *51*, 3881.
(50) Smith, W. E. *J. Org. Chem.* **1972**, *37*, 3972.
(51) Nandi, L. G.; Nicoleti, C. R.; Stock, R. I.; Barboza, T. A.; Andreaus, J.; Machado, V. G. *Spectrochim. Acta, Part A* **2015**, *136*, 1600.
(52) Becke, A. D. *Phys. Rev. A: At., Mol., Opt. Phys.* **1988**, *38*, 3098.
(53) Perdew, J. P. *Phys. Rev. B: Condens. Matter Mater. Phys.* **1986**, *33*, 8822.
(54) Grimme, S.; Antony, J.; Ehrlich, S.; Krieg, H. *J. Chem. Phys.* **2010**, *132*, 154104.
(55) Weigend, F.; Ahlrichs, R. *Phys. Chem. Chem. Phys.* **2005**, *7*, 3297.
(56) Neese, F. *Wiley Interdisciplinary Reviews: Computational Molecular Science* **2012**, *2*, 73.
(57) Weinhold, F.; Landis, C. R. *Chem. Educ. Res. Pract.* **2001**, *2*, 91.
(58) Schmidt, M. W.; Baldridge, K. K.; Boatz, J. A.; Elbert, S. T.; Gordon, M. S.; Jensen, J. H.; Koseki, S.; Matsunaga, N.; Nguyen, K. A.; Su, S.; Windus, T. L.; Dupuis, M.; Montgomery, J. A. *J. Comput. Chem.* **1993**, *14*, 1347.
(59) *SADABS, APEX2, and SAINT*; Bruker AXS Inc.: Madison, WI, 2009.
(60) Sheldrick, G. M. *Acta Crystallogr., Sect. A: Found. Crystallogr.* **2008**, *64*, 112.
(61) Spek, A. L. *J. Appl. Crystallogr.* **2003**, *36*, 7.

DOI: 10.1021/acs.joc.5b00983
J. Org. Chem. 2015, 80, 7971−7983